Ryszka et al. *Int. J. Mass. Spectrom.* 396 (2016) 48

Dissociative multi-photon ionization of isolated uracil and uracil-adenine complexes

M. Ryszka[1], R. Pandey[1], C. Rizk[1,2], J. Tabet[2], B. Barc[1], M. Dampc[1,3], N.J. Mason[1], S. Eden*[1]

[1] Dept. of Physical Sciences, The Open University, Walton Hall, Milton Keynes, MK7 6AA, United Kingdom

[2] Dept. of Physics, Faculty of Sciences II, Lebanese University, Fanar – Maten, Lebanon

[3] Dept. of Physics of Electronic Phenomena, Gdańsk University of Technology, 80-952 Gdańsk, Poland

* Corresponding author: s.p.eden@open.ac.uk

Abstract

Recent multi-photon ionization (MPI) experiments on uracil revealed a fragment ion at m/z 84 that was proposed as a potential marker for ring opening in the electronically excited neutral molecule. The present MPI measurements on deuterated uracil identify the fragment as $C_3H_4N_2O^+$ (uracil$^+$ less CO), a plausible dissociative ionization product from the theoretically predicted open-ring isomer. Equivalent measurements on thymine do not reveal an analogous CO loss channel, suggesting greater stability of the excited DNA base. MPI and electron impact ionization experiments have been carried out on uracil-adenine clusters in order to better understand the radiation response of uracil within RNA. Evidence for $C_3H_4N_2O^+$ production from multi-photon-ionized uracil-adenine clusters is tentatively attributed to a significant population of π-stacked configurations in the neutral beam.

Graphical Abstract

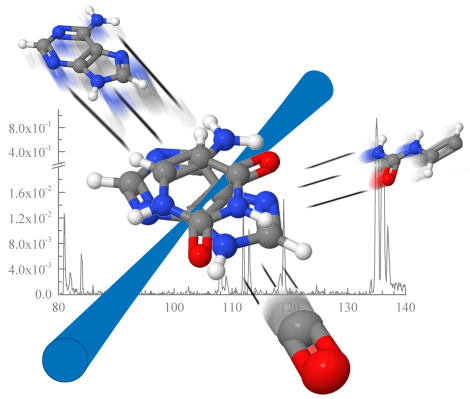

Highlights

UV multi-photon ionization measurements on deuterated uracil have identified a CO loss pathway that may indicate ring opening in the electronically excited neutral molecule. The first dissociative ionization experiments on uracil-adenine complexes have revealed that the CO loss channel is also accessible in these clusters.

Keywords: Uracil; adenine-uracil clusters; fragmentation; multi-photon ionization; electron impact ionization; mass spectrometry

1. Introduction

The dynamics and stabilities of nucleobases following excitation to their bright $S_2(\pi\pi^*)$ states have been researched intensively in recent years [1]. Time resolved pump-probe experiments [2] and calculations [3] on isolated molecules have yielded rich insights into their excited state dynamics, while studies of base pairs and hydrated clusters have enabled closer analogies to be drawn with cellular environments [4]. Internal conversion to the vibrationally hot electronic ground state (either directly or via S_1 states of mainly $n\pi^*$ and $\sigma\pi^*$ character) dominates $S_2(\pi\pi^*)$ deactivation [5, 6], although intersystem crossing to long-lived triplet states has also been identified [7, 8]. The present work investigates dissociative multi-photon ionization (MPI) of uracil ($C_4H_4N_2O_2$) as a tool to gain additional understanding of its relaxation pathways from $S_2(\pi\pi^*)$ and from excited ionic states. Uracil forms two hydrogen bonds with adenine in RNA and is geometrically similar to the DNA base thymine ($C_5H_6N_2O_2$; uracil methylated at the C5 site of the pyrimidine ring system).

Structural modifications and bond breaking in electronically excited or ionized DNA and RNA bases are of particular interest as they represent potential radiation damage pathways in the respective macromolecules. Nachtigallova et al. [9] theoretically identified ring-opening at the $S_2(\pi\pi^*)$-$S_1(\sigma(n\text{-}\pi)\pi^*)$ crossing seam. More recently, Richter et al. [10] carried out dynamical calculations with non-adiabatic and spin-orbit couplings that supported this pathway. The ring-opening process was predicted to lead to new photochemical products [9]. Barc et al. [11] observed a new fragment ion at m/z 84 ($uracil^+$ minus CO or CNH_2) by single-color 2-photon ionization of uracil. The threshold photon energy (5.29 ± 0.06 eV) for this product agreed with the calculated energy (5.25 eV at CASSCF level) of the ring-opening crossing seam [9] and the geometry of the predicted isomer indicates likely CO abstraction. Therefore MPI production of this fragment ion was proposed as a potential experimental marker for ring opening in neutral excited uracil, suggesting possibilities for diverse measurements exploring the process in depth (e.g. using coincidence and / or time-resolved methods). The first aim of the present work was to test if the new fragment ion is indeed due to CO loss by studying MPI of deuterated uracil (dominantly $C_4D_4N_2O_2$). These results have the added value of identifying several previously debated fragments from the radical cation, while further evidence to assign specific peaks is provided by high-resolution MPI mass spectra. The paper also presents equivalent MPI measurements on thymine, for which no analogous ring-opening process has been predicted [9]. A distinctly higher pump energy (5.64 eV, 220 nm) was applied than in the previous MPI studies of thymine (4.34-4.77 eV, 285.7-260 nm) [6, 12, 13, 14, 15, 16, 17], increasing the likelihood of isomeric transitions during radiationless deactivation. Finally, MPI and electron impact ionization (EII) experiments were carried out on uracil-adenine clusters as a step towards better understanding the dissociative ionization pathways of uracil within RNA. Whereas several spectroscopic studies have been carried out on adenine-thymine complexes in supersonic beams [18, 19, 20], to our knowledge no previous experiments on isolated uracil-adenine clusters have been reported in the literature.

2. Experimental

The experimental system has been described in detail by Barc et al. [11]. Briefly, argon or helium buffer gas (0.5-1.2 bar) seeded with sublimated uracil, thymine, adenine (all Sigma-Aldrich with stated purity ≥99%) and / or deuterated uracil (CDN isotopes, 98.4%) flowed continuously through a 50 μm diameter pinhole into a pumped chamber (500 ls^{-1} in the Fig. 1-4 measurements; 1,000 ls^{-1} in Fig. 5) to form a supersonic jet. The powder temperatures (250-277°C) were comparable with or lower than those applied in previous supersonic beam experiments that reported no evidence for thermally driven decomposition, isomerization, or reactivity of uracil, adenine, or thymine [21]. The carrier gas pressure, the powder temperature, and the pumping speed in the expansion chamber were modified in order to gain control over the level of clustering in the jet. However the greatest effect was achieved by changing the carrier gas; the experiments in helium expansions showed no evidence for clustering. The jet passed through a skimmer into a second pumped chamber and crossed an Nd:YAG pumped and frequency doubled dye laser beam (*Continuum Powerlight II 8000* - *Sirah Cobra-Stretch*, repetition rate 10 Hz, pulse width 7 ns, pulse energy 100-2,000 μJ, wavelength 219-277 nm). A commercial electron gun (*Kimball ELG-2*) provided an alternative ionizing beam. The resulting ions were detected using a reflectron time-of-flight (TOF) mass spectrometer (supplied by KORE Technology and shown schematically in Fig. 1a) with the *field free region* held at -2 kV. The pre-amplified ion signals were timed using a *Fast Comtec P7887* time-to-digital conversion (TDC) card with a minimum bin size of 250 ps. The data acquisition system was based on a *LabView* application interfacing with the TDC card and a laser pulse energy meter (*Spectrum Detector SPJ-D-8*).

The average laser pulse energy was adjusted using the delay between the pulses triggering the xenon flash lamps and the *Q-switch* of the Nd:YAG laser. A convex lens on a slider was used to modify the laser spot diameter at the interaction with the molecular beam and hence control the fluence. This was previously estimated using simple ray diagrams for partially defocused measurements [11, 22] but we did not have a reliable method to determine the spot diameter close to the focal point. This problem was solved by recording MPI signals as a function of the voltage on the reflection electrode (see Fig.1). For non-dissociative ionization (zero kinetic energy release), the key condition for detection was that the voltage at the point in space where the ion was produced should be closer to ground than the voltage on the reflection electrode (the reflection voltage). If not, the ion would hit the electrode and would not be reflected towards to detector. Hence, the reflection voltage did not affect the ion signal significantly in Fig. 1b until it corresponded to the crossing position of the focused laser spot and the molecular beam. In order to convert the reflection voltage range across which the ion signal fell from its maximum to zero into a measure of the laser spot diameter, the electric field between the grounded backplate and the extraction grid (-380 V, 13.0 mm from the backplate) was simulated using CPO-3D software.

3. Results and Discussion

3.1. MPI comparisons of gas-phase uracil, deuterated uracil, and thymine

Fig. 2 compares high-mass ion production from gas-phase uracil (U), deuterated uracil, and thymine (T). The conditions of the target beam (helium seeded with molecules sublimated at 250 °C) and the focused laser beam parameters were the same in all three measurements. No cluster ion peaks were observed. The absence of any signals attributable to protonated nucleobases provides further evidence of negligible clustering in the neutral beams since such species have previously been identified as major dissociation products of nucleobase cluster ions. For example, protonated uracil was detected strongly in an MPI study of hydrated uracil clusters [11] and electronic structure calculations have shown that the hydrogen-bonded uracil dimer cation relaxes to a proton-transferred form [23]. Similarly, thermochemical calculations have shown that proton transfer from T^+ to T in a dimer cation is exothermic [24, 25]. The (nucleobase ion + 1 mass unit) / (nucleobase ion) signal ratios in Fig. 2 are 6±1% for U and 5±1% for T, in good agreement with the respective natural isotope ratios of 5.2% and 6.3% [26].

The ratio of the peaks at m/z 116 and 115 in Fig. 2b indicates that the molecular beam comprised 80% $C_4D_4N_2O_2^+$ and 20% $C_4D_3HN_2O_2^+$. Rice et al. [29] studied electron impact ionization of various pyrimidine derivatives, including partially deuterated uracil produced by dissolution in D_2O. They assumed that replacement of hydrogen by deuterium occurred exclusively at nitrogen atoms. Accordingly, we expect that our brief exposure of fully deuterated uracil to air (to load the sample in the experiment) led to some hydrogen / deuterium exchange at nitrogen sites. The m/z 88 and 87 peaks in Fig. 2b clearly indicate the loss of 28 mass units from $C_4D_4N_2O_2^+$ and $C_4D_3HN_2O_2^+$. This effectively rules out assigning the m/z 84 peak in Fig. 2a to CNH_2 loss from uracil$^+$. As the loss of two nitrogen atoms (or an N_2 molecule) without further fragmentation would require a very unlikely rearrangement, we assign the peak to CO loss. This is a highly plausible product following the N3-C4 fissure predicted by Nachtigallova et al. [9]. Accordingly, the present high-resolution data (table 1) shows that the Gaussian-fitted m/z value agrees more closely with $C_3H_4N_2O^+$ (CO loss) than $C_4H_4O_2^+$ (N_2 loss) or $C_3H_2NO_2^+$ (CNH_2 loss).

As discussed in the introduction, our particular interest in the MPI production of m/z 84 ions from uracil stems from their proposed association with ring opening at the crossing seam of the neutral molecule's two lowest-lying singlet excited states [11]. This fragment ion is not formed by direct excitation of gas-phase uracil to ionic states, for example in single collisions with electrons or ions [27]. Aside from MPI with a pump wavelength ≤232 nm [11], m/z 84 ions from uracil have only been observed in laser-induced plasmas (266 and 1064 nm ns-timescale pulses) [28] where multiple collisions can plausibly lead to the ionization of excited neutral isomers. As previous electron impact ionization and single photon ionization mass spectra of gas-phase thymine did not produce $C_4H_6N_2O^+$ (m/z 98, T^+ minus

CO) [29, 30][*], any MPI production of this fragment ion could suggest an analogous excited state ring-opening pathway. Plot c in Fig. 2 shows no evidence for $C_4H_6N_2O^+$ production. Accordingly, Nachtigallova et al. [9] noted the absence of a ring-opening channel in the calculated relaxation dynamics of thymine following S_2 excitation [2]. The reasons for this specific difference compared with uracil were not discussed, although possible kinematic effects of the CH_3 group of thymine were mentioned in the context of more general differences in the excited molecules' relaxation pathways.

3.2. Low-mass fragment ion production from uracil$^+$ and deuterated uracil$^+$

The MPI production of fragment ions with m/z ≤ 75 from uracil and deuterated uracil is shown in Fig. 3. The comparison identifies several fragment ions whose attribution has been debated in the literature (notably CH_2^+, CNH_2^+, and $C_2H_2O^+$), while further evidence to assign specific peaks is provided by a high-resolution MPI mass spectrum of uracil (summarized in table 1). Gaussian fits were generated using Origin 8.5.1 software to determine the centers of the time-of-flight peaks and the mass calibration was preformed with reference to the C^+ and uracil$^+$ (m/z 112.027 [26]) peaks.

Starting at low masses, the first aspect of Fig. 3 to note is the absence of any signal at m/z 13 in the deuterated measurement. CH^+ ions were produced from uracil, both in the present data (albeit weakly) and in previous MPI and EII experiments [11, 31]. The fact that CH^+ ions were not produced from the deuterated target (approximately 80% $C_4D_4N_2O_2$ and 20% $C_4D_3HN_2O_2$) suggests that the hydrogen atoms were localized on nitrogen sites only. Ion production at m/z 14 has been attributed to CH_2^+ by Imhoff et al. [31] and N^+ by Jochims et al. [30]. The present high-resolution measurement shows that CH_2^+ dominates. Accordingly the strong peaks at m/z 14 and 16 in Fig. 3b can be assigned to CD^+ and CD_2^+.

The most striking result in the next ion group (m/z 24-32) is the shift of the strongest peak from m/z 28 in the uracil mass spectrum (Fig. 3a) to m/z 30 in the deuterated uracil measurement (Fig. 3b). This clearly indicates that the peaks are respectively dominated by CH_2N^+ and CD_2N^+, whereas Imhoff et al. [31] assigned this feature to CO^+. The present high-resolution measurement (Fig. 4 and table 1) also rules out attributing the peak to CO^+ production. As weak C_2H^+ production was previously observed from uracil [11, 31], the peak at m/z 26 in Fig. 3b is expected to contain C_2D^+. However, comparing the magnitude the m/z 25 feature in Fig. 3a with the m/z 26 peak in both plots suggests an additional contribution of CN^+ (not proposed in any previous works). The peaks at m/z 28-30 in Fig. 3b are expected to contain contributions of $C_2D_2^+$ and CDN^+, as well as possibly $CHDN^+$, CO^+, and CDO^+. The only plausible assignment for the clear feature at m/z 32 in the deuterated measurement is

[*] Fig. 2 does not include an MPI mass spectrum of cytosine because a fragment ion at m/z 83 (the radical cation m/z value minus 28 mass units) has been reported in previous electron impact ionization experiments [29].

CD_3N^+, removing previous doubt regarding the origin of the m/z 29 peak in the uracil mass spectrum [30].

The most intense peak in the m/z 38-45 group is shifted from m/z 42 in the uracil measurement (Fig. 3a) to m/z 44 in the deuterated uracil result (Fig. 3b). This supports the assignment of these peaks to $C_2H_2O^+$ / $C_2D_2O^+$ [30, 32, 33], as opposed to $C_2H_4N^+$ / $C_2D_4N^+$ [31, 33]. The group's second strongest peak (m/z 40 from uracil) is also apparently shifted by two mass units in the deuterated measurement, consistent with its accepted assignment to $C_2H_2N^+$ / $C_2D_2N^+$. The main peaks in the m/z 67-74 group are also consistent with the previous assignments to $C_3H_2NO^+$ and $C_3H_3NO^+$ from uracil [30, 32, 33]. It is interesting to note that Fig. 3a shows a broad *tail* structure extending 0.3 μs (approximately 2 m/z units in this part of the calibrated mass spectrum) after the m/z 69 peak. Our previous work demonstrated uracil$^+$ dissociation to $C_3H_3NO^+$ in the TOF field free region (1.3–14.6 μs after ionization). The present tail can be attributed to the same metastable dissociation taking place while uracil$^+$ is accelerated from the laser/molecular beam crossing point to the entrance of the TOF field free region (a journey time of 1.1 μs in the present measurements).

3.3. Uracil clusters and uracil-adenine clusters

Fig. 5 compares MPI and EII measurements carried out on uracil (plots a and b) and on a beam containing both uracil and adenine (plots c and d). The latter was achieved by loading the powder cartridge with an equal mixture of uracil and adenine. Increased pumping speed was applied in these experiments to enhance clustering. Examination of the remaining powder after the experiments and no unexplained peaks in the mass spectra supported the absence of thermally driven reactivity.

Strong production of UH^+ relative to U^+ in Fig. 5a-d shows that the target beams contained significant numbers of clusters. The most stable uracil dimer configuration features two parallel N3H•••OC2 bonds (see insert in Fig. 2a for conventional numbering of the ring atoms) [34, 35]. MPI mass spectra of pure uracil clusters have previously been measured using 274 nm ns-timescale laser pulses but no information on fragment ions was reported [36]. The only experiment in the literature that probed fragment ion production from pure uracil clusters was performed for 100 keV O^{5+} impact ionization [37] with an aggregation source that produced larger clusters than the present apparatus. In this ion irradiation experiment, signals at m/z 83 (U^+ minus HCO) and 95 (U^+ minus OH) were interpreted as providing evidence for hydrogen bonding. The present MPI and EII measurements did not reveal ion production at these m/z values above the background level.

To our knowledge, no previous experiments have probed fragment ion production from uracil-adenine clusters. The stability of the optimized hydrogen-bonded UA pair (-0.76 eV) is similar to AA (-0.81 eV) and UU (-0.76 eV) [38] so mixed clusters are expected to form a significant part of the target beam. No new species were detected; the fragment ions in Figs. 5c and 5d have been observed previously from dissociated uracil$^+$ (e.g. $C_3H_3NO^+$ at m/z 69 [11]), adenine$^+$ (e.g. $C_4H_4N_4^+$ at m/z 108 [39]), and / or protonated adenine (e.g. $C_4H_5N_4^+$ at m/z 109 [40]). In view of our particular interest in the MPI

production of $C_3H_4N_2O^+$ (m/z 84 with its proposed link to excited-state ring opening), it is noteworthy that this ion signal approximately doubled in the uracil-adenine measurement compared with the pure uracil result (0.021±0.003 counts per pulse in Fig 5c compared with 0.011±0.002 in Fig 5a). No peak at m/z 84 has been observed from isolated, clustered, or protonated adenine [22, 37, 39, 40], or from protonated uracil [41]. The fact that the U^+ signals were the same (to within the uncertainty limits) in plots a and c as well as in plots b and d suggests that this result was not simply due to different populations of isolated uracil molecules in the neutral beams. Therefore the result supports $C_3H_4N_2O^+$ production from multi-photon ionized uracil-adenine complexes. Zhanpeisov and Leszczynski [42] and Martinez [43] calculated that the most stable uracil-adenine configuration involves one (U) N3H•••N1 (A) bond and one (U) C4O•••HC6 (A) bond. Considering the proximity of these bonds to the proposed N3-C4 rupture site, the formation of hydrogen-bonded UA pairs is expected to have a suppressive effect on the uracil ring opening process identified by Nachtigallova et al. [9]. Hence the present results can be rationalised by supposing that the target beam contained a range of uracil-adenine configurations including π-stacked complexes in which excited state ring opening is more plausible. It is interesting to note that the interaction energy of the optimized UA stacked pair is -0.44 eV, compared with -0.36 eV for its pure uracil counterpart [38]. Therefore, we suggest that the enhanced MPI production of $C_3H_4N_2O^+$ in the adenine-uracil measurement compared with the pure uracil result may be traced to the relative populations of π-stacked clusters in the neutral beams.

The U^+/A^+ signal ratio was 71% in Fig. 5d, very close to the 75% ratio between the calculated EII cross sections [43]. This indicates similar target densities of the two molecules in the expansion, as expected from the reported vapor pressures [44]. However the MPI signal of A^+ was around 80 times stronger than U^+ (Fig. 5c). Kutor et al.'s [45] time-resolved pump (262 nm) - probe (780 nm) measurements on gas-phase adenine and uracil showed that parent ion production could be fitted by summing a fast decay component (time constant 100 fs for A^+, 70 fs for U^+) and a slow decay component (1.14 ps for A^+, 2.15 ps for U^+). Importantly, the slow decay amplitude / the fast decay amplitude was 95% for A^+, compared with 9% for U^+. Therefore the intense MPI production of A^+ compared with U^+ in Fig. 5c can be partially explained by relatively efficient access to slow deactivation routes from S_2 (notably internal conversion to S_0 via S_1) in adenine. Adenine's lower ionization energy [30] is expected to further increase its MPI efficiency in the present laser beam conditions, while access to triplet states [46, 10, 8] can also play a role. Additionally, the A^+ signal may be enhanced by MPI via long-lived exciplex states in π-stacked nucleobases [1, 47].

Li et al. [48] stated that proton transfer from N3 on adenine to N1 on uracil is expected in UA^+. This expectation appears to be based on analogies with other pyrimidine-purine radical cations, notably the Watson-Crick pairs [49]. The stabilities of UA^+ with and without proton transfer are not available in the literature, nor are any associated reaction barriers. If Li et al.'s [48] expectation is correct and there is no barrier to prevent fast proton transfer then UH^+ would be a major dissociative ionization product of UA. However, Fig. 5 shows that the UH^+ signals were reduced significantly in the present measurements on uracil-adenine compared with pure uracil. Once again, this result is consistent with

the neutral beam containing a range of mixed cluster configurations including π-stacked complexes as well as hydrogen-bonded base pairs. Specific calculations on UA cluster ions and experiments with greater control of target cluster configurations (for example, exploiting Zeeman or Stark selection methods [50]) are required to clarify the proton transfer processes.

4. Conclusions

The present measurements on deuterated uracil have provided unambiguous assignments for a number of fragment ions from uracil that have been debated in the literature. In particular, the multi-photon ionization product at m/z 84 has been identified as $C_3H_4N_2O^+$ (uracil$^+$ less CO). This is consistent with a recently proposed interpretation [11] linking the fragment ion to a theoretically-predicted ring-opening process at the $S_2(\pi\pi^*)$-$S_1(\sigma(n\text{-}\pi)\pi^*)$ crossing seam [9]. No equivalent ring-opening pathway has been predicted in excited thymine and accordingly the present MPI measurements on thymine did not reveal an analogous CO loss channel. Crossed beam experiments have been carried out on uracil-adenine clusters for the first time. MPI measurements provided evidence for enhanced $C_3H_4N_2O^+$ production from uracil-adenine clusters compared with pure uracil clusters. As the formation of hydrogen-bonded UA pairs is expected to suppress the proposed uracil ring opening process, this may indicate a significant presence of π-stacked complexes in the neutral beam.

Acknowledgements

The authors are grateful for the expert technical support provided by F. Roberston, C. Hall, and their colleagues at the OU. The OU's financial and logistical support is also acknowledged. S.E. acknowledges the support the British EPSRC through a Life Sciences Interface Fellowship (EP/E039618/1), a Career Acceleration Fellowship (EP/J002577/1), and a Research Grant (EP/L002191/1). The European Commission is acknowledged for a Marie Curie Intra-European Reintegration Grant (MERG-CT-2007-207292).

References

[1] K. Kleinermanns, D. Nachtigallová, M. S. de Vries. *Int. Rev. Phys. Chem*, 32(2), 308–342, 2013.

[2] H. R. Hudock, B. G. Levine, A. L. Thompson, H. Satzger, D. Townsend, N. Gador, S. Ullrich, A. Stolow, T. J. Martnez. *J. Phys. Chem. A*, 111(34), 8500–8508, 2007.

[3] B. P. Fingerhut, K. E. Dorfman, S. Mukamel. *J. Chem. Theory Comput.*, 10(3), 1172–1188, 2014.

[4] T. Gustavsson, Á. Bányász, E. Lazzarotto, D. Markovitsi, G. Scalmani, M. J. Frisch, V. Barone, R. Improta. *J. Am. Chem. Soc.*, 128(2), 607–619, 2006.

[5] S. Yamazaki, T. Taketsugu. *J. Phys. Chem. A*, 116(1), 491–503, 2012.

[6] S. Ullrich, T. Schultz, M. Z. Zgierski, A. Stolow. *J. Am. Chem. Soc.*, 126(8), 2262–2263, 2004.

[7] Y. He, C. Wu, W. Kong. *J. Phys. Chem. A*, 108(6), 943–949, 2004.

[8] M. Ligare, F. Siouri, O. Bludsky, D. Nachtigallova, M. S. de Vries. *Phys. Chem. Chem. Phys.*, 17, 24336–24341, 2015.

[9] D. Nachtigallová, A. J. A. Aquino, J. J. Szymczak, M. Barbatti, P. Hobza, H. Lischka. *J. Phys. Chem. A*, 115(21), 5247–5255, 2011.

[10] M. Richter, S. Mai, P. Marquetand, L. González. *Phys. Chem. Chem. Phys.*, 16(44), 24423–24436, 2014.

[11] B. Barc, M. Ryszka, J. Spurrell, M. Dampc, P. Limão-Vieira, R. Parajuli, N. J. Mason, S. Eden. *J. Chem. Phys.*, 139(24), 244311, 2013.

[12] H. Kang, K. T. Lee, B. Jung, Y. J. Ko, S. K. Kim. *J. Am. Chem. Soc.*, 124(44), 12958–12959, 2002.

[13] E. Samoylova, T. Schultz, I. Hertel, W. Radloff. *Chemical Physics*, 347(1-3), 376–382, 2008.

[14] J. Gonzalez-Vazquez, L. Gonzalez, E. Samoylova, T. Schultz. *Phys. Chem. Chem. Phys.*, 11, 3927–3934, 2009.

[15] C. Canuel, M. Mons, F. Piuzzi, B. Tardivel, I. Dimicoli, M. Elhanine. *J. Chem. Phys.*, 122(7), 074316, 2005.

[16] B. B. Brady, L. A. Peteanu, D. H. Levy. *Chem. Phys. Lett.*, 147(6), 538–543, 1988.

[17] M. Schneider, R. Maksimenka, F. J. Buback, T. Kitsopoulos, L. R. Lago, I. Fischer. *Phys. Chem. Chem. Phys.*, 8, 3017–3021, 2006.

[18] C. Plützer, I. Hünig, K. Kleinermanns, E. Nir, M. S. de Vries. *ChemPhysChem*, 4(8), 838–842, 2003.

[19] N. Gador, E. Samoylova, V. R. Smith, A. Stolow, D. M. Rayner, W. Radloff, I. V. Hertel, T. Schultz. *J. Phys. Chem. A*, 111(46), 11743–11749, 2007.

[20] K. B. Bravaya, O. Kostko, S. Dolgikh, A. Landau, M. Ahmed, A. I. Krylov. *J. Phys. Chem. A*, 114(46), 12305–12317, 2010.

[21] P. Colarusso, K. Zhang, B. Guo, P. F. Bernath. *Chem. Phys. Lett.*, 269(1-2), 39–48, 1997.

[22] B. Barc, M. Ryszka, J.-C. Poully, E. J. A. Maalouf, Z. el Otell, J. Tabet, R. Parajuli, P. van der Burgt, P. Limão-Vieira, P. Cahillane, M. Dampc, N. Mason, S. Eden. *Int. J. of Mass Spectrom.*, 365-366, 194–199, 2014.

[23] A. A. Zadorozhnaya, A. I. Krylov. *J. Chem. Theory Comput.*, 6(3), 705–717, 2010.

[24] M. Liu, T. Li, F. S. Amegayibor, D. S. Cardoso, Y. Fu, J. K. Lee. *J. Org. Chem.*, 73(23), 9283–9291, 2008.

[25] C. L. Stumpf. *Application of Fourier transform ion cyclotron resonance mass spectrometry to a mechanistic study, examination of the properties of nucleobase radical cations, and chemical ionization reagent development*. PhD thesis, Purdue University, Indiana, USA, 2000.

[26] J. J. Manura, D. J. Manura, *Scientific Instrument Services Isotope Distribution Calculator*, http://www.sisweb.com/mstools/isotope.htm, accessed 2015.

[27] B. Coupier, B. Farizon, M. Farizon, M. Gaillard, F. Gobet, N. de Castro Faria, G. Jalbert, S. Ouaskit, M. Carré, B. Gstir, G. Hanel, S. Denifl, L. Feketeova, P. Scheier, T. D. Märk. *Eur. Phys. J. D*, 20(3), 459–468, 2002.

[28] I. Lopez-Quintas, M. Oujja, M. Sanz, A. Benitez-Cañete, C. Hutchison, R. de Nalda, M. Martin, R. Ganeev, J. Marangos, M. Castillejo. *Applied Surface Science*, 302, 299–302, 2014.

[29] J. M. Rice, G. O. Dudek, M. Barber. *J. Am. Chem. Soc.*, 87(20), 4569–4576, 1965.

[30] H.-W. Jochims, M. Schwell, H. Baumgärtel, S. Leach. *Chemical Physics*, 314, 263–282, 2005.

[31] M. Imhoff, Z. Deng, M. A. Huels. *Int. J. of Mass Spectrom.*, 262, 154–160, 2007.

[32] S. Matsika, C. Zhou, M. Kotur, T. C. Weinacht. *Faraday Discuss.*, 153, 247–260, 2011.

[33] L. Sadr-Arani, P. Mignon, H. Abdoul-Carime, B. Farizon, M. Farizon, H. Chermette. *Phys. Chem. Chem. Phys.*, 14, 9855–9870, 2012.

[34] M. Pitonák, K. E. Riley, P. Neogrády, P. Hobza. *ChemPhysChem*, 9(11), 1636–1644, 2008.

[35] P. Hobza, J. Šponer. *Chemical Reviews*, 99(11), 3247–3276, 1999.

[36] N. J. Kim, H. Kang, G. Jeong, Y. S. Kim, K. T. Lee, S. K. Kim. *Proceedings of the National Academy of Sciences*, 98(9), 4841–4843, 2001.

[37] T. Schlathölter, F. Alvarado, S. Bari, A. Lecointre, R. Hoekstra, V. Bernigaud, B. Manil, J. Rangama, B. Huber. *ChemPhysChem*, 7(11), 2339–2345, 2006.

[38] N. Ding, X. Chen, C.-M. L. Wu, H. Li. *Phys. Chem. Chem. Phys.*, 15, 10767–10776, 2013.

[39] P. J. van der Burgt, S. Finnegan, S. Eden. *Eur. Phys. J. D*, 69(7), 173, 2015.

[40] N. R. Cheong, S. H. Nam, H. S. Park, S. Ryu, J. K. Song, S. M. Park, M. Perot, B. Lucas, M. Barat, J. A. Fayeton, C. Jouvet. *Phys. Chem. Chem. Phys.*, 13, 291–295, 2011.

[41] L. Sadr-Arani, P. Mignon, H. Chermette, T. Douki. *Chemical Physics Letters*, 605-606, 108–114, 2014.

[42] N. U. Zhanpeisov J. Leszczynski. *J. Phys. Chem. A*, 102(30), 6167–6172, 1998.

[43] A. Martnez. *J. Phys. Chem. A*, 113(6), 1134–1140, 2009.

[44] J. Tabet, S. Eden, S. Feil, H. Abdoul-Carime, B. Farizon, M. Farizon, S. Ouaskit, T. D. Märk. *Phys. Rev. A*, 82, 022703, 2010.

[45] M. Kotur, T. Weinacht, C. Zhou, S. Matsika. *IEEE Journal of Selected Topics in Quantum Electronics*, 18(1), 187–194, 2012.

[46] S. Ullrich, T. Schultz, M. Z. Zgierski, A. Stolow. *Phys. Chem. Chem. Phys.*, 6, 2796–2801, 2004.

[47] T. Takaya, C. Su, K. de La Harpe, C. E. Crespo-Hernández, B. Kohler. *Proceedings of the National Academy of Sciences*, 105(30), 10285–10290, 2008.

[48] X. Li, Z. Cai, M. D. Sevilla. *J. Phys. Chem. A*, 106(40), 9345–9351, 2002.

[49] J. Bertran, A. Oliva, L. Rodrguez-Santiago, M. Sodupe. *J. Am. Chem. Soc.*, 120(32), 8159–8167, 1998.

[50] S. Trippel, Y.-P. Chang, S. Stern, T. Mullins, L. Holmegaard, J. Küpper. *Phys. Rev. A*, 86(3), 033202, 2012.

[51] J. Rejnek, M. Hanus, M. Kabelác, F. Ryjácek, P. Hobza. *Phys. Chem. Chem. Phys.*, 7, 2006–2017, 2005.

[52] R. N. Casaes, J. B. Paul, R. P. McLaughlin, R. J. Saykally, T. van Mourik. *J. Phys. Chem. A*, 108(50), 10989–10996, 2004.

Figure 1: (a) Schematic diagram of the reflectron mass spectrometer and (b) MPI measurements (220 nm, He 0.8 bar, powder 264 °C) of uracil$^+$ production as a function of the reflection voltage. The signal cut-off width (9±1 V) can be directly correlated to the diameter (0.31±0.04 mm) of the focused laser spot at the intersection with the molecular beam.

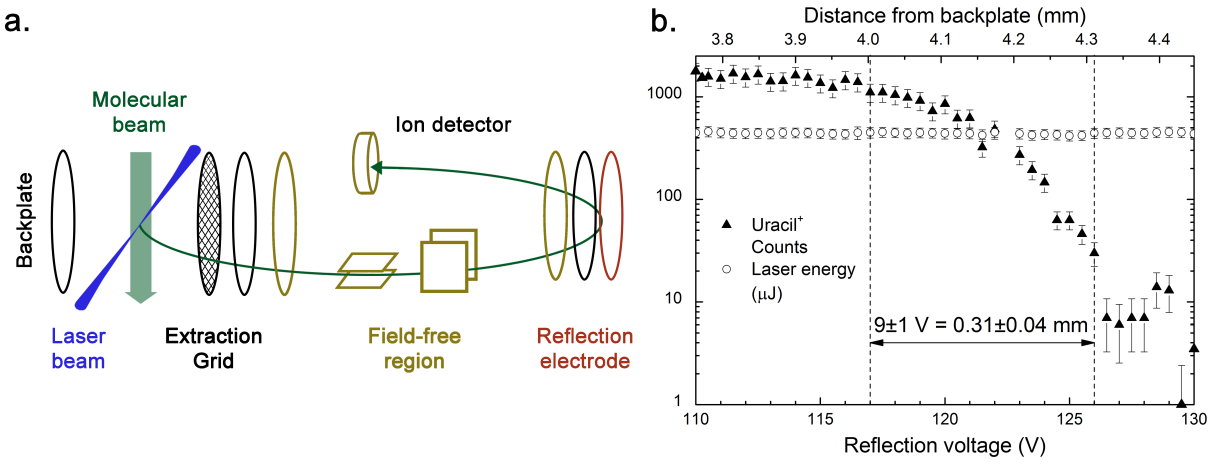

Figure 2: MPI mass spectra (220 nm, average fluence 9×10^{7} Wcm^{-2}, He 0.8 bar, powder 250 °C) of uracil, deuterated uracil, and thymine: details of the m/z ranges close to the parent ion masses. The grey dashed line corresponds to the parent ion minus 28 mass units. The dominant gas-phase tautomers are the diketo forms shown in the inserts [51, 21, 52]. The bold dashed line on uracil signifies the neutral ring fissure position at the S_2-S_1 crossing seam based on Nachtigallova et al.'s [9] calculations.

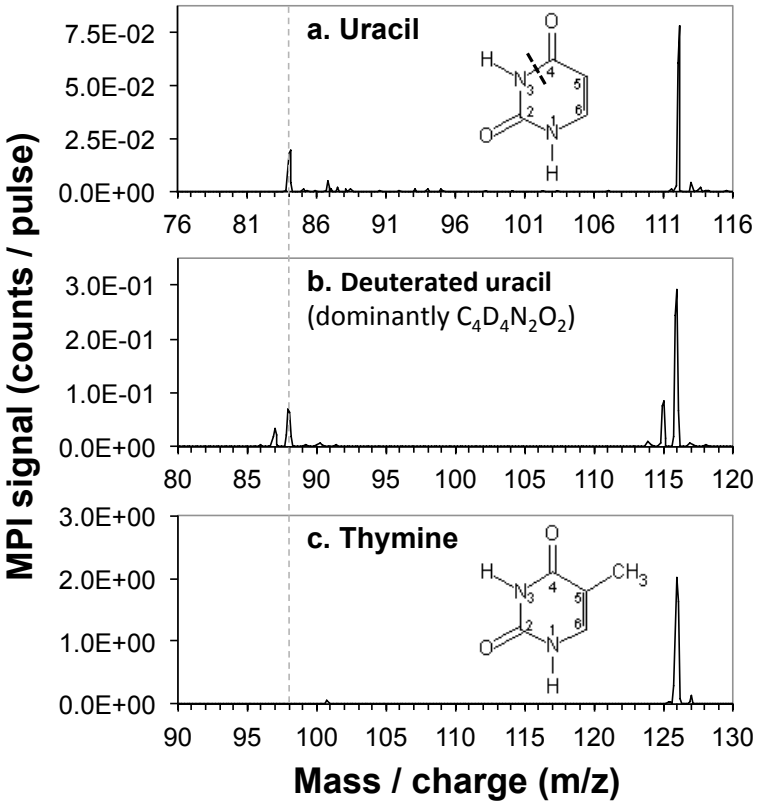

Figure 3: MPI mass spectra (220 nm, average fluence 9×10^7 Wcm^{-2}, He 0.8 bar, powder 250 °C) of uracil and deuterated uracil: detail of the m/z range 10-75. The peak assignments discussed in the text have been labeled.

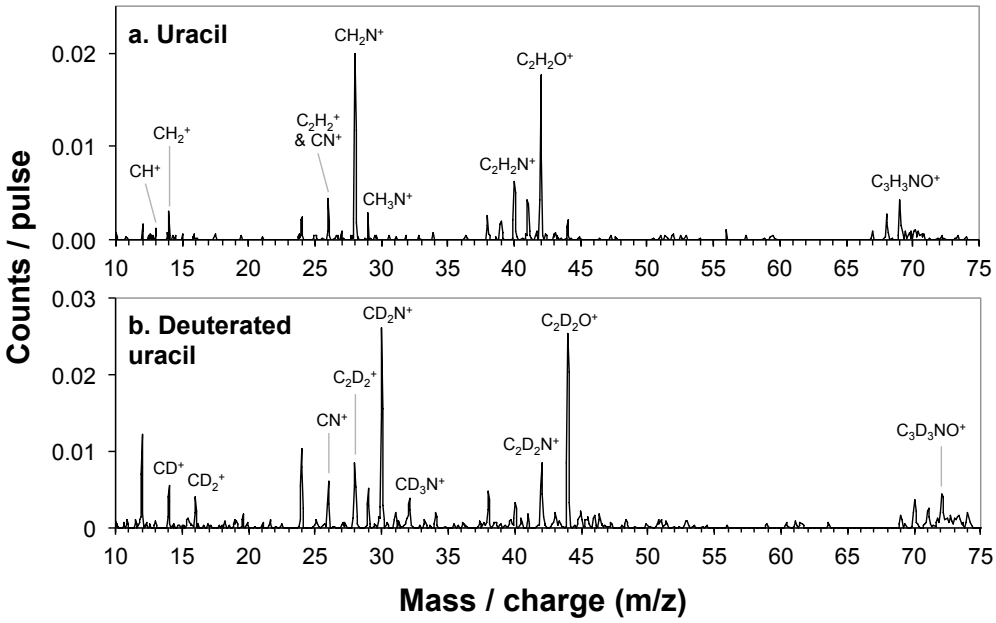

Figure 4: MPI of uracil (220 nm, average fluence 9×10^{7} Wcm^{-2}, Ar 1.2 bar, powder 277°C) recorded with minimum time bin widths (250 ps): detail of fragment ion peak at m/z ~ 28.

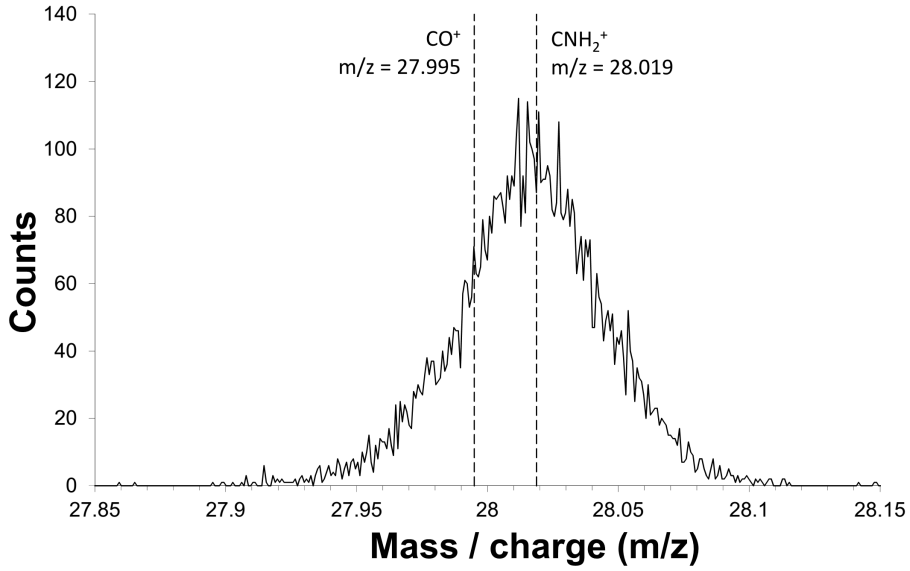

Figure 5: MPI mass spectra (220 nm, average fluence 9×10^{7} Wcm^{-2}) and EII (200 eV) of uracil (plots a and b) and a mixture of uracil and adenine (plots c and d) vaporized at 270 °C in 1.0 bar of argon.

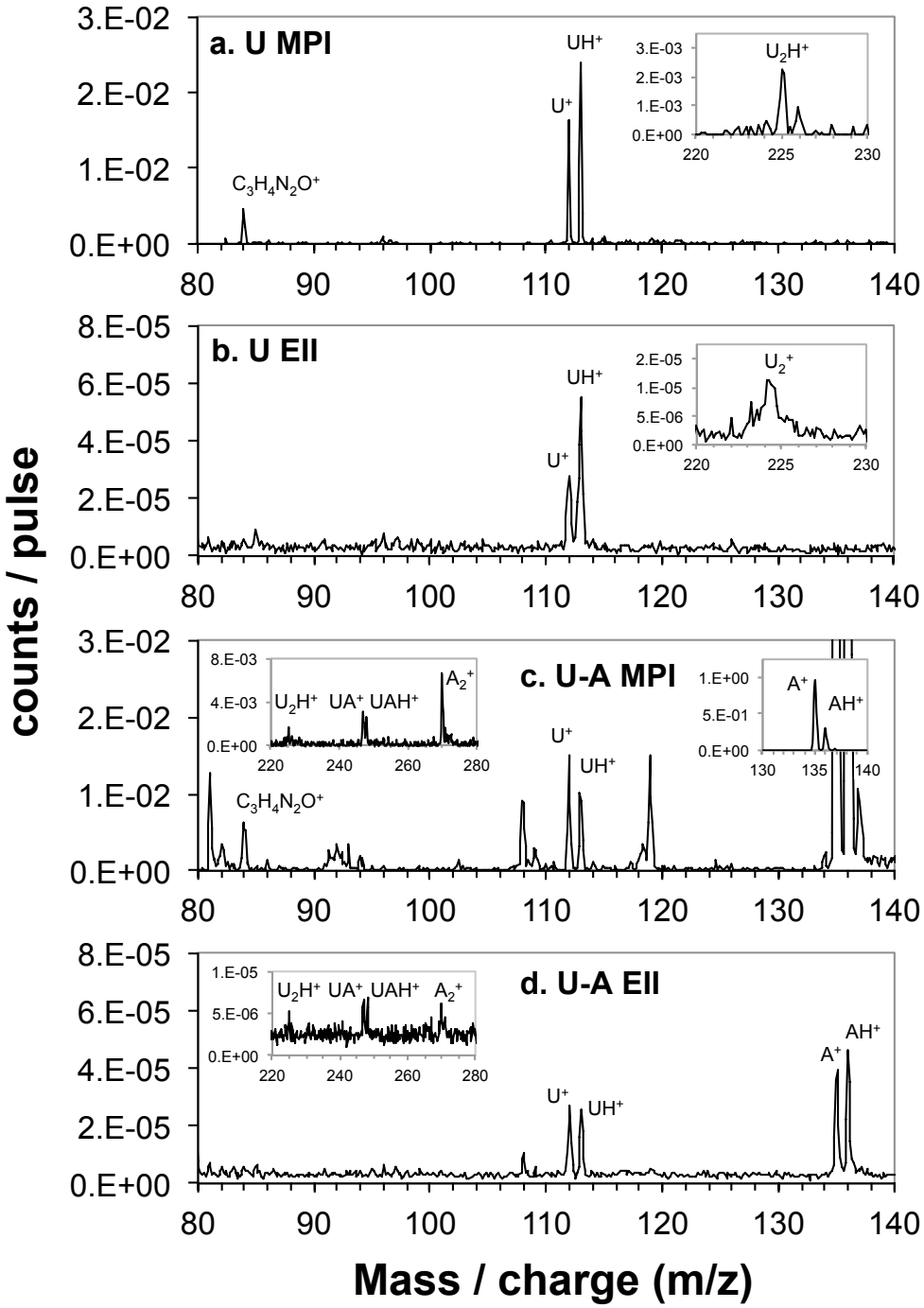

Table 1: Summary of the high-resolution TOF data for uracil MPI (see Fig. 4).

Gaussian center (m/z) & % of strongest peak [A, B]	Possible ions with previous assignments	Mass (AU) of possible ions [26]	Notes
113.033 ± 0.013, 13%	$C_4H_5N_2O_2^+$ $C_4H_4N_2O_2^+$ (1x ^{13}C)	113.035 113.031	Combination
112.027 ± 0.010, 44%	$C_4H_4N_2O_2^+$	112.027	Calibration reference
84.049 ± 0.011, 17%	$C_3H_4N_2O^+$ [11] $C_4H_4O_2^+$ $C_3H_2NO_2^+$	84.032 84.021 84.009	Deuterated comparison supports $C_3H_4N_2O^+$
44.000 ± 0.009, 10%	$C_2H_4O^+$ CH_2NO^+ [31] CO_2^+	44.026 44.014 43.990	Possible combination
43.004 ± 0.010, 7%	$C_2H_3O^+$ $CHNO^+$ [30]	43.018 43.006	
42.007 ± 0.007, 28%	$C_2H_4N^+$ [31, 33] $CH_2N_2^+$ $C_2H_2O^+$ [30, 32, 33] CNO^+	42.034 42.022 42.011 41.998	Deuterated comparison supports $C_2H_2O^+$
41.016 ± 0.008, 10%	$C_2H_3N^+$ [30, 32] CHN_2^+ C_2HO^+ [30]	41.027 41.014 41.003	Possible combination
40.018 ± 0.007, 16%	$C_3H_4^+$ $C_2H_2N^+$ [30] CN_2^+ C_2O^+	40.031 40.019 40.006 39.995	Deuterated comparison supports $C_2H_2N^+$
39.008 ± 0.010, 6%	$C_3H_3^+$ C_2HN^+	39.024 39.011	
38.001 ± 0.008, 8%	$C_3H_2^+$ C_2N^+	38.016 38.003	
29.019 ± 0.006, 18%	CH_3N^+ [30, 33] HN_2^+ HCO^+ [30]	29.027 29.014 29.003	Deuterated comparison supports CH_3N^+
28.013 ± 0.005, 100%	C_2H_4+ CH_2N^+ [30, 32, 33] N_2^+ CO^+ [31]	28.031 28.019 28.006 27.995	Deuterated comparison supports CH_2N^+
27.003 ± 0.008, 10%	$C_2H_3^+$ CHN^+ [30]	27.023 27.011	
26.009 ± 0.006, 17%	$C_2H_2^+$ [30] CN^+	26.016 26.003	Deuterated comparison supports a CN^+ contribution
24.011 ± 0.006, 14%	C_2^+	24.000	
14.013 ± 0.004, 24%	CH_2^+ [31] N^+ [30]	14.016 14.003	Deuterated comparison supports CH_2^+
13.005 ± 0.004, 18%	CH^+	13.008	
12.000 ± 0.002, 36%	C^+	12.000	Calibration reference

[A] The table only includes peaks with intensities >5% of the most intense peak (m/z 28). Further weak peaks were observed at m/z 1 (H^+), 15 (CH_3^+ [31]), 16 (CH_4^+, H_2N^+, or O^+), 25 (C_2H^+), 45 (CH_3NO^+ or CHO_2^+), 68 ($C_3H_2NO^+$ [30]), 69 ($C_3H_3NO^+$ [7, 5, 6]), 70 ($C_3H_4NO^+$ [30, 33]), and 85 ($C_3H_5N_2O^+$ or $C_3H_3NO_2^+$).

[B] The uncertainty estimations on the Gaussian center values are based on summing the uncertainties given by the fitting software (Origin 8.5.1) and the uncertainty based on the calibration.